

Structure-activity Relationship under Vibrational Strong Coupling

Thabassum Ahammad N K

MS15110

*A dissertation submitted for the partial fulfilment of
BS-MS dual degree in Science*



Department of Chemical Sciences
Indian Institute of Science Education and Research Mohali

December 2020

Certificate of Examination

This is to certify that the dissertation titled “Structure-activity Relationship under Vibrational Strong Coupling” submitted by Mr. Thabassum Ahammad N K (Reg.No. MS15110) for the partial fulfilment of BS-MS dual degree programme of the Institute, has been examined by the thesis committee duly appointed by the Institute. The committee finds the work done by the candidate satisfactory and recommends that the report be accepted.



Dr. Sugumar Venkataramani

Dr. P. Balanarayan

Dr. Jino George

(Supervisor)

Declaration

The work presented in this dissertation has been carried out by me under the guidance of Dr. Jino George at the Indian Institute of Science Education and Research Mohali. This work has not been submitted in part or in full for a degree, a diploma, or a fellowship to any other university or institute. Whenever contributions of others are involved, every effort is made to indicate this clearly, with due acknowledgement of collaborative research and discussions. This thesis is a bonafide record of original work done by me and all sources listed within have been detailed in the bibliography.

Thabassum Ahammad N K

(Candidate)

Dated:

In my capacity as the supervisor of the candidate's project work, I certify that the above statements by the candidate are true to the best of my knowledge.

A handwritten signature in black ink, appearing to be 'J. George', written over a diagonal line.

Dr. Jino George
(Supervisor)

Acknowledgments

Words often fail to pay one's gratitude. Still, I would like to convey my sincere gratitude to the beautiful humans who aided and extended their backing in this fruitful endeavour.

First and foremost, I owe a deep sense of gratitude to my thesis supervisor Dr Jino George for providing me with a spectacular opportunity. His constant inspiration, timely suggestions and meticulous scrutiny helped me enormously in accomplishing this task. He has been incredibly supportive throughout the voyage. Moreover, his persistence in solving problems and dedication towards his students always inspired me. Thank you for making this journey fabulous.

I am grateful to my committee members, Dr Sugumar Venkataramani and Dr P Balanarayan, for giving valuable suggestions to complete this project.

It is a genuine pleasure to express my gratefulness to Ms Jyothi Lather for acting as a source of inspiration and being with me always. Her prompt suggestions with enthusiasm and dynamism aided me a lot in completing this work. I want to express my deep sense of gratitude to Pooja, Jaibir, Akhila, Kuljeet, Jhuma, Chithra, Atul, Parvathi and Yashika for facilitating a marvellous atmosphere in the lab.

I want to express immense gratitude to my friends, who were there with me always. I am grateful to my parents who taught me kindness, generosity, patience and above all, how to manage success and failures. Furthermore, I am grateful to the beautiful humans who joined for endless coffee sessions. Last but not least, I would like to acknowledge the IISER community for facilitating a remarkable opportunity to craft my skillsets.

List of figures

Figure 1.1 Illustration of two masses connected with springs to form coupled oscillator.

Figure 1.2 A) Interaction of a two-level system to form upper polaritonic state (UP) and lower polaritonic state (LP) as described in Jaynes-Cummings (JC) model. B) Interaction of two-level systems to form upper polaritonic state (UP) and lower polaritonic state (LP) as well as N-1 dark states according to Tavis-Cummings (TC) model.

Figure 1.3 Interaction of molecular resonance and cavity resonance to form polaritonic states.

Figure 1.4 Illustration of the dispersive nature of the strong coupling phenomena. E_C , E_M denotes the energy curves of cavity and matter states, respectively. P_+ is the upper polaritonic state and P_- is the lower polaritonic state. $\hbar\Omega_R$ denotes the Rabi splitting.

Figure 1.5 Illustration of the molecular ensemble with refractive index n confined in an FP cavity with mirrors m_1 and m_2 separated by length L .

Figure 2.1 Illustration of a reaction confined under strong coupling condition. M_1 and M_2 are the two mirrors used to create the state of strong coupling.

Figure 2.2 (a) Evolution of the transmission spectra of the system over time. As the isomerisation reaction proceeds, it can be noted that the cavity mode at 560 nm splits into two and evolves further. (b) Kinetic plot of the reaction when the system is at ON-resonance condition and (c) at OFF-resonance condition. The figure is reprinted from [21].

Figure 2.3 (a) Schematic diagram of vibrational strong coupling. b) Deprotection reaction PTA TBAF (c) IR transmission spectrum of PTA manifesting the coupling at 860 cm^{-1} d) Modification of reaction kinetics through the evolution of cavity modes in various conditions. The figure is reprinted from [22]

Figure 2.4 Schematic illustration of the vibrational strong coupling phenomenon which forms new vibro-polaritonic states.

List of tables

Table 3.1 C=O stretching frequency of the benzoate esters.

Table 3.2 Melting point of the molecules synthesized.

Table 3.3 C=O stretching frequency of the solvents involved in the study.

Table 3.4 Apparent rate constants for the solvolysis of esters in the non-cavity condition.

Table 3.5 Substituent constant values used in Hammett plot.

Table 3.6 FSR in isopropyl acetate before and after injection in ON-resonance condition.

Table 3.7 Apparent rate constants for the solvolysis in isopropyl acetate under non-cavity and cavity condition.

Abbreviations

CQED- Cavity Quantum Electrodynamics

VSC - Vibrational Strong Coupling

USC - Ultra- Strong Coupling

ESC - Electronic Strong Coupling

TBAF - tetra-n-butylammonium fluoride

F-P cavity - Fabry-Pérot Cavity

J-C model - Jaynes- Cummings model

T-C model - Tavis - Cummings model

FWHM - Full width half maximum DMF - Dimethylformamide

FSR - Free spectral range

Contents

| | |
|--|-----------|
| List of figures..... | IV |
| List of tables..... | V |
| Abbreviations | VI |
| Abstract..... | 2 |
| 1. Theoretical Insights of Strong Light-matter Coupling | 3 |
| 1.1. Introduction..... | 4 |
| 1.2. Experimental Evolution..... | 5 |
| 1.3. Theoretical Underpinnings..... | 5 |
| 1.4. Coupling Regimes | 9 |
| 1.5. Optical Cavity..... | 10 |
| 1.6. Transfer Matrix Method..... | 11 |
| 2. Controlling Chemical Reactions under Vibrational Strong Coupling | 12 |
| 2.1. Polaritonic Chemistry..... | 13 |
| 2.2. Vibrational Strong Coupling..... | 16 |
| 2.3. Cavity Catalysis and Cooperativity..... | 17 |
| 3. Experimental Aspects and Implications | 18 |
| 3.1. Structure Activity Relationship and Hammett Plot..... | 19 |
| 3.2. Experimental Setup..... | 21 |
| 3.3. Synthesis of para-Nitrophenyl Benzoate Esters..... | 21 |
| 3.4. Solvent Systems..... | 24 |
| 3.5. Solvolysis of the benzoate Esters..... | 25 |
| 3.6. Results and Discussions..... | 26 |
| 3.7. Conclusions..... | 32 |
| 4. Bibliography | 34 |
| 5. Appendix A | 37 |

Abstract

Very recently, vibrational strong coupling (VSC) was used as a tool to modify chemical reaction rates by coupling the reactant in the confined medium of a microfluidic cavity. This concept is called polaritonic chemistry. This is a novel and unconventional approach for controlling reaction rate and has better selectivity as the cavity modes can be tuned precisely to target a given vibrational band. Understanding the mechanism of polaritonic chemistry is a challenging task as it involves light and matter as components. Few experimental and theoretic studies are available in the literature that show the effect of ON resonance coupling of vibrational band to modify chemical reaction rates. However, some of the reactions are accelerated and some others are deaccelerated while coupling selected vibrational states. As of now, a clear microscopic picture is not yet available to understand the process of polaritonic chemistry. Achieving insight into the underlying concepts of the reaction mechanism of polaritonic chemistry can help to design experiments with high efficiency, that can replace the conventional protocols of chemical reaction control.

In the current thesis, we focus on the effect of structure-activity relationship to follow a simple ester hydrolysis under VSC. Here, we used cooperative VSC, i.e., coupling a solvent vibration that is overlapping with reactant vibrational state to modify the chemical reaction rate. The phenomenon of cavity catalysis is utilized by selecting different ester molecules with varying substitution and followed their linear free energy relationship under strong coupling condition. The current study is a small step towards understanding the unusual behaviour of chemical reaction rates in strong coupling chemistry.

Theoretical Insights of Strong Light-matter Coupling

An overview of strong light-matter interaction, experimental and theoretical progress and underlying theoretical concepts are discussed here. The chapter starts with introducing strong light-matter interaction and its background and further extend towards discussing experimental evolution and theoretical understanding. The chapter ends with a discussion on transfer matrix method.

1.1 Introduction

The study of matter-matter and light-matter interaction is essential for understanding the existence of Nature. In general, these interactions are mainly classified into weak and strong interactions. For example, weak matter-matter interactions like dispersion forces as well as strong interactions like ionic bonding can overturn the properties of the associated systems. Weak light-matter interactions can affect the spontaneous emission process in fluorescing molecules called as Purcell effect.¹ Whereas, strong light-matter interaction can reshuffle the energy of the coupled states along with new features that are unique to the hybrid light-matter states. Cavity Quantum Electrodynamics (CQED) deals with strong light-matter interaction with an atom and electromagnetic field in a confined mode. CQED is approximated to a simple two-level emitter interacting with a photonic mode. Serge Haroche and Daniel Kleppner championed the field CQED through their revolutionary experiments which manifested that it is indeed possible to tune the property of spontaneous emission when an excited atom is placed inside an optical cavity.²

Hybrid light-matter entity is a state-of-the-art perception on the ideas of strong light-matter interaction. Hybrid light-matter states are generated by exploiting the concept of vacuum field confined and placing matter inside an optical cavity. In quantum electrodynamics point of view, it's argued that there is no such thing as an absolute vacuum. In addition, the existence of the vacuum field is validated with experiments like Casimir effect³ and lamb shift.⁴ Conventionally, in molecular orbital hybridization, we can control the physicochemical properties of various molecules predominantly through tailoring the types of atoms involved and the bonding between the atoms in a compound. Nevertheless, it has been shown that hybrid light-matter states can alter the physicochemical properties of molecules and materials in a similar fashion, but here the other component will be light.⁵ When the cavity mode of the vacuum electromagnetic field is coupled to molecular transition, they produce hybrid light-matter states known as polaritonic states. Polaritonic states are formed when light-matter coupling dominates in all the possible relaxation pathways. Here, more precisely, the coupling regimes can be again split up into weak, strong and ultra-strong coupling regimes.⁵ In this thesis, we will be particularly focusing on strong coupling regime. A system is said to be in the strong coupling regime when the rate of exchange of energies between the coupled entities are faster than any dissipation process in the system. Dissipations from the system can arise from various sources like scattering, cavity lifetime, and spontaneous emission.

1.2 Experimental Evolution

The first experimental investigation in the strong coupling regime was done by G. N. Zhizhin et. al in 1975.⁶ They studied the surface polariton splitting by coupling the thin film local oscillator vibrations. This was followed by various studies of strong coupling phenomenon over different systems.^{2,7,8}

The first experimental investigation to observe hybrid light-matter state characteristics in strong coupling between light and molecule was carried by Pockard et.al in 1982.⁹ Later in 1998, Lidzey et al. demonstrated that anthracene crystal could be probed under strong coupling condition in organic semiconductor microcavity¹⁰. In 2008, Naomi J Halas et. al investigated the coupling of plasmons of a nano-shell and the exciton of a molecular J-aggregate to obtain hybridized plasmon-exciton states.¹¹

1.3 Theoretical Understanding

Classically, strong coupling can be explained with the concept of coupled oscillators. When two undamped oscillators are coupled to form a combined single system, exchange of energy happens between the individual systems. Consider two masses m_1 and m_2 connected with springs with spring constants k_1 and k_2 (figure 1.2). The masses are interconnected with another spring with spring constant k_c . Frequency of the oscillators are ω_1 and ω_2 . When the system attains resonance condition ($\omega_1 = \omega_2$), the system accomplish strong coupling state to generate two new normal modes with an energy separation. This phenomenon of generating new normal modes through strong coupling is observed in acoustic waves as well.¹²

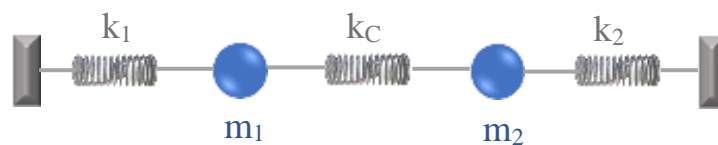


Figure 1.1 Illustration of two masses connected with springs to form coupled oscillator.

Semi classically, Rabi model explains the light-matter interaction considering a quantum mechanical two-level atomic system and classical electromagnetic field approach.^{13,14}

To explain the strong coupling phenomenon further, we need to understand the interaction of electromagnetic field with molecules. Light constitutes perpendicularly oscillating electric and magnetic fields. The oscillating electric field component interacts with fluctuating electronic cloud of the atom or molecule to produce absorption and emission

transitions which we detect using various spectroscopic methods. The probability for a transition to occur between an initial state ψ_i and final state ψ_f^* can be elucidated from the following transition dipole moment integral,

$$\mu_T = \int \psi_f^* \hat{\mu} \psi_i d\tau$$

where $\hat{\mu}$ is the electric dipole moment operator. A non-zero transition dipole moment integral indicates non-zero interaction energy and this interaction facilitates a probable transition. From this, we extend our discussion towards the quantum mechanical models to explain the strong coupling phenomenon.

In 1963, the pioneering work of Jaynes and Cummings in quantum optics theoretically established the phenomenon of strong coupling for the first time.¹⁵ The Jaynes-Cummings (JC) model consider a two-level system interacting with optical cavity mode of a quantized electromagnetic field. JC model envisages the eigenstates of the coupled system as a combination of individual light and matter states, explicitly lower (LP) and upper (UP) polaritonic states. Within the rotating wave approximation, the total Hamiltonian for the JC model is a sum of individual Hamiltonians from the cavity mode, atom and the interaction between them. Total Hamiltonian of the JC model is written as follows,

$$\begin{aligned} \hat{H}_{JC} &= \hat{H}_{cav} + \hat{H}_{mol} + \hat{H}_{int} \\ \hat{H}_{JC} &= \frac{1}{2} \hbar \omega \hat{\sigma}_z + \hbar \omega_c (\hat{a}^\dagger \hat{a} + \frac{1}{2}) + \hbar g_0 (\hat{a}^\dagger \hat{\sigma}_- + \hat{a} \hat{\sigma}_+) \end{aligned}$$

where ω and ω_c represents the frequencies of molecular and cavity transitions, respectively. \hat{a}^\dagger and \hat{a} are the field creation and field annihilation operators, respectively. $\hat{\sigma}_z$ takes care of the energies of the states, $\hat{\sigma}_+$ is the raising operator denoting the transition from ground to excited state and $\hat{\sigma}_-$ is the lowering operator denoting transition from excited to ground state.

$$\sigma_z = \begin{pmatrix} 1 & 0 \\ 0 & -1 \end{pmatrix}, \sigma_+ = \begin{pmatrix} 0 & 1 \\ 0 & 0 \end{pmatrix}, \sigma_- = \begin{pmatrix} 0 & 0 \\ 1 & 0 \end{pmatrix}$$

The extent of coupling between molecule and cavity is denoted with g_0 . Energy exchange between the molecule and cavity can be interpreted from the interaction Hamiltonian of the aforementioned equation. Although JC model could explain the coupling between the two-level system and cavity mode, however, it is restricted to a single molecule.

Further developments to JC model considering N molecules within rotating wave approximation, Tavis-Cummings (TC) model, also known as Dicke model came up. In Dicke

model, N molecules interact with a single cavity mode to form lower (LP) and upper (UP) polaritonic states and $N-1$ dark states where N is the number of two-level atomic systems involved. The interaction between the two-level atoms and cavity mode using a Holstein Primakoff transformation happens in terms of the following Hamiltonian,

$$\hat{H}_{TC} \cong \hbar\omega \left(-\frac{N}{2} + \hat{b}^\dagger \hat{b} \right) + \hbar\omega_c \hat{a}^\dagger \hat{a} + \hbar g (\hat{a}^\dagger \hat{b} + h.c.),$$

where \hat{b} is bosonic operator, g is the shared coupling constant, and h.c is the Hermitian conjugate. The shared coupling constant, which takes the form of $g = g_0\sqrt{N}$ indicates how the overall coupling strength depends on the concentration of molecules. An illustration of both JC and TC model is shown in figure 1.3.

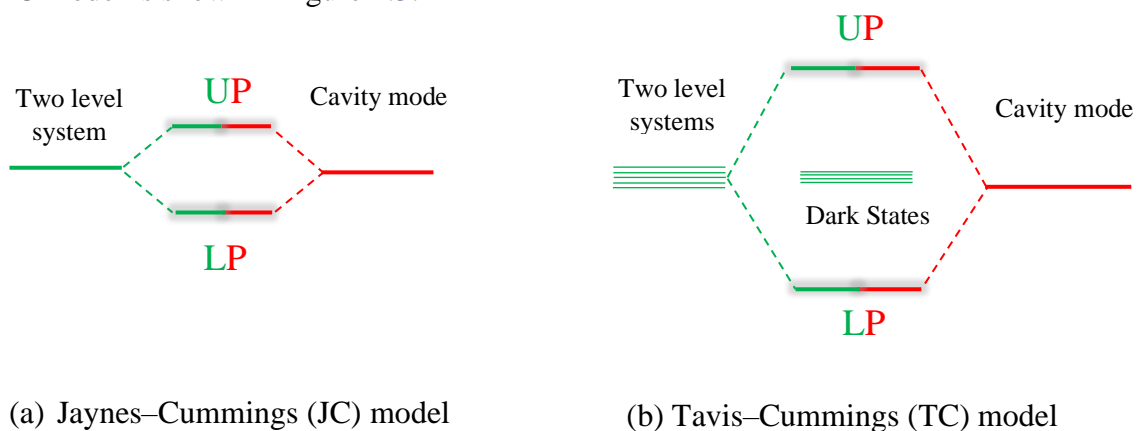


Figure 1.2 (a) Interaction of a two-level system to form upper polaritonic state (UP) and lower polaritonic state (LP) as described in Jaynes-Cummings (JC) model. (b) Interaction of two-level systems to form upper polaritonic state (UP) and lower polaritonic state (LP) as well as $N-1$ dark states according to Tavis-Cummings (TC) model.

Exploiting the TC model and using Hopfield – Bogoliubov method, the newly formed hybrid states can be described with the following wave functions,

$$|P + \rangle = c_{11} |e\rangle_m |0\rangle_c + c_{12} |g\rangle_m |1\rangle_c$$

$$|P - \rangle = c_{22} |e\rangle_m |0\rangle_c + c_{21} |g\rangle_m |1\rangle_c$$

where $P+$ and $P-$ denotes upper and lower polaritonic states respectively. These wave functions are composed as a linear combination of the molecule in the excited state (e) with zero (0) photons in the cavity and the molecule in the ground state (g) with one (1) photon in the cavity.

The newly formed polaritonic states are separated by Rabi splitting energy $\hbar\Omega_R$,

$$\hbar\Omega_R = 2d \cdot E_0 = 2d \sqrt{\frac{\hbar\omega}{2\varepsilon_0 v}} \times \sqrt{n_{ph} + 1}$$

where d is the transition dipole moment of the molecule, E_0 is the electric component of the electromagnetic field, $\hbar\omega$ is the resonant energy, ε_0 is the vacuum permittivity, v is the volume of the electromagnetic mode, and n_{ph} is the number of photons involved in coupling. The equation mentioned above clearly establish that it is indeed possible to have a Rabi splitting energy even when there is no photon ($n_{ph}=0$) involved in the process. This energy is known as vacuum Rabi splitting energy. An illustration of the interaction between molecular resonance and cavity resonance forming polaritonic states separated by rabi splitting energy is shown in figure 1.3.

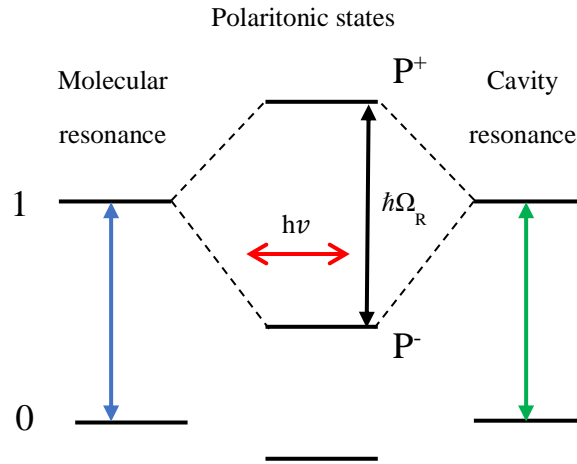


Figure 1.3 Interaction of molecular resonance and cavity resonance to form polaritonic states.

Dispersive nature of hybrid light-matter states is a salient feature of the strong coupling regime which is a contribution from the photonic part. When the system is uncoupled, energy curves of the two states exhibit a converging nature (figure 1.4). In contrary, when there is a coupling between the two states in strong coupling regime, energy curves exhibit a diverging nature. The smallest energy separation between the diverged energy curves is considered as Rabi splitting energy. Dispersion curves can be plotted using the following equation,

$$k_{\parallel} = \frac{2\pi}{\lambda} \sin \theta$$

where k_{\parallel} is the in-plane wave vector, λ is wavelength of the light and θ is the angle of incidence.

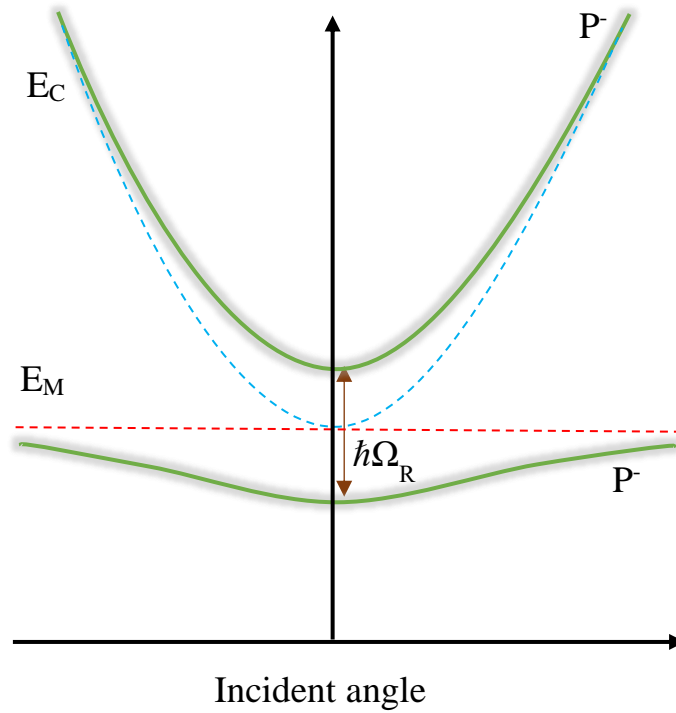


Figure 1.4 Illustration of the dispersive nature of the strong coupling phenomena. E_C , E_M denotes the energy curves of cavity and matter states, respectively. $P+$ is the upper polaritonic state and $P-$ is the lower polaritonic state. $\hbar\Omega_R$ denotes the Rabi splitting.

1.4 Coupling Regimes

Based on the strength of the light-matter coupling, the coupling regimes can be divided into weak, strong, and ultra-strong coupling regime. In weak coupling regime, Purcell effect modifies the emission rate of electronic transitions of the matter.¹⁶ A system is said to be in strong coupling regime when the magnitude of the Rabi splitting is larger than the full width at half max (FWHM) of both the molecular and optical cavity resonances. Mathematically, strong coupling regime is achieved when $2g > \left(\frac{\gamma+k}{2}\right)$ where g , γ and k denotes coupling strength, non-resonant decay rate of the molecule and photon decay rate of optical cavity, respectively. In ultra-strong coupling (USC) regime, the Rabi splitting is enormous in juxtaposition with individual transition frequencies and shows aberrations from Jaynes-Cummings model.^{17, 17b} USC can modify features like work function and phase transitions.¹⁸

1.5 Optical Cavity

Predominantly, feasible geometries used in molecular strong coupling is Fabry-Perot cavities or Plasmonic modes due the low-quality factor (vide-infra) that match with the molecular transitions. The experimental setup we use in our study to obtain vibrational strong coupling condition is a Fabry-Perot (FP) cavity tuned in the infrared region, which is a simplest form of an optical cavity. FP cavity consist of two parallel mirrors placed closely in which the distance between them can be adjusted. The mirrors are arranged in such a way that the standing waves are confined in between with a given frequency of vibration.

The cavity is said to be in ON-resonance condition when the system obey the following relation presupposing that no additional photons are invaded into the cavity,

$$L_{cav} = m \left(\frac{\lambda}{2n} \right)$$

where λ is the wavelength of light, n is the refractive index of the system studied inside the cavity, and m is an integer. The quality of a cavity formed can be assessed with an expression called quality factor which can be expressed as below,

$$Q = \frac{\omega_r}{\Delta\omega_c}$$

where ω_r is the frequency of the resonant and $\Delta\omega_c$ is the FWHM of the cavity mode generated.

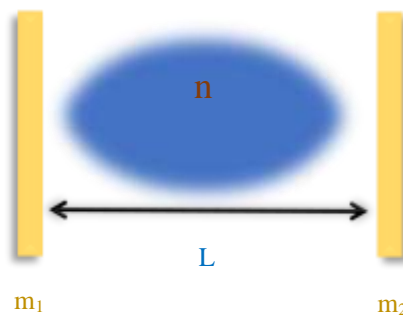


Figure 1.5 Illustration of the molecular ensemble with refractive index n confined in an FP cavity with mirrors m_1 and m_2 separated by length L .

We couple the molecular ensemble in an FP cavity to obtain Rabi splitting. The electronic or vibrational modes of the ensemble is coupled to cavity mode generated in the FP cavity. To achieve the coupling experimentally, the molecular ensemble with refractive index n is placed in between the two parallel mirrors m_1 and m_2 separated by a length L (Figure 1.5).

To facilitate the coupling, we tune the cavity modes to match with the transition from molecular ensemble. Frequency difference or free spectral range (FSR) between two successive cavity modes can be obtained from the following equation,

$$k(\text{cm}^{-1}) = \frac{10000}{2nL}$$

1.6 Transfer Matrix Method

One of the most widely used theoretical method to validate the experimental result of strong coupling in optical microcavities is transfer matrix method (TMM).^{19, 20} TMM is a semi-classical electrodynamics approach based on Maxwell's equation in continuous media. The behaviour of light at the interface is taken into account by Fresnel equations. Moreover, TMM assumes a uniform refractive index for each layer considered. This assumption affects the accuracy in describing the matter part despite the fact that TMM provides accurate description for light part. Mostly, Fabry-Perot cavity systems are modelled using TMM method. Dispersion relation, reflectance spectra, transmittance spectra, and phase correlation diagram etc. can be simulated using TMM.¹⁹⁻²⁰

Controlling Chemical Reactions under Vibrational Strong Coupling

A brief discussion on Polaritonic Chemistry is carried out in this chapter. Major experimental studies that contributed to strong light-matter interaction studies are discussed. Furthermore, a brief description on Vibrational Strong Coupling is also provided. The chapter ends with a discussion on the notion of cooperativity and cavity catalysis.

2.1 Polaritonic Chemistry

Polaritonic chemistry is an exciting interdisciplinary field bringing together the concepts in quantum optics and molecular science to modulate various properties and reactivity of chemical systems.⁵ The concept of polaritonic states to influence the chemical reactivity of organic molecules is established by revolutionary experiments from the group of Thomas Ebbesen.^{21, 22} A schematic illustration of a reaction confined under strong coupling condition is shown in figure 2.1.

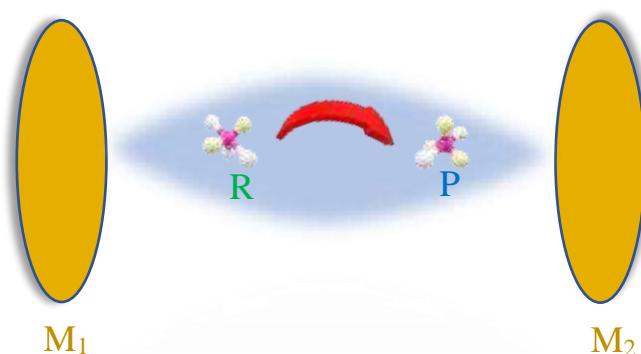


Figure 2.1 Illustration of a reaction confined under strong coupling condition. M_1 and M_2 are the two parallel mirrors used to create the state of strong coupling.

The pioneering experimental work from the group of Ebbesen²¹ which coupled electronic transitions to cavity mode launched new avenue for the field of polaritonic chemistry. Thereafter, an ever-growing interest is witnessed in the field of polaritonic chemistry from various experimental and theoretical groups all over the globe. Ebbesen et al. demonstrated that it is certainly possible to alter the chemical reaction landscapes by coupling the electronic transition to cavity modes of vacuum electromagnetic field generated inside an optical cavity. They probed the photoisomerization reaction between spiropyran and merocyanine isomers inside an optical cavity and manifested modifications in chemical reaction rates. Plots involved in this study are incorporated in figure 2.2. Modifications in the photochemical reaction rate are validated theoretically by taking stilbene and azobenzene molecule as a model system.

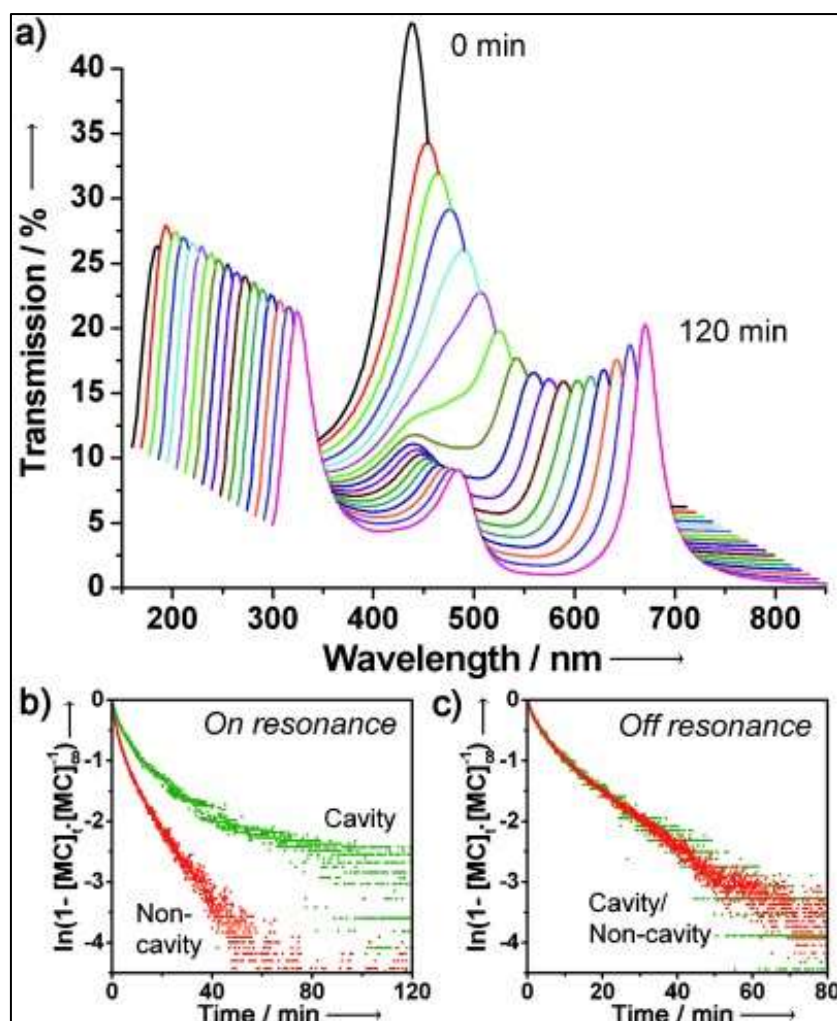


Figure 2.2 (a) Evolution of the transmission spectra of the system over time. As the isomerisation reaction proceeds, it can be noted that the cavity mode at 560 nm splits into two and evolves further. (b) Kinetic plot of the reaction when the system is at ON-resonance condition and (c) at OFF-resonance condition. The figure is reprinted from [21].

Moreover, the study discussed above, which coupled electronic transitions to cavity mode triggered the idea of coupling vibrational transitions to cavity modes in an optical cavity. Striking to this explicit possibility of coupling to vibrational transitions, in 2016 Ebbesen's group probed the ground state deprotection of 1-phenyl-2-trimethylsilylacetylene (PTA) with tetra-n-butylammonium fluoride (TBAF) by coupling the vibrational transitions to cavity modes.²² The stretching frequency corresponding to C-Si bond is coupled to the cavity mode by tuning the resonant cavity. Under these conditions, the reaction exhibited a decreased reaction kinetics by a factor of 5.5 with respect to non-cavity condition (Figure 2.3). Furthermore, thermodynamic results indicated a shift from associative to the dissociative type transition state.

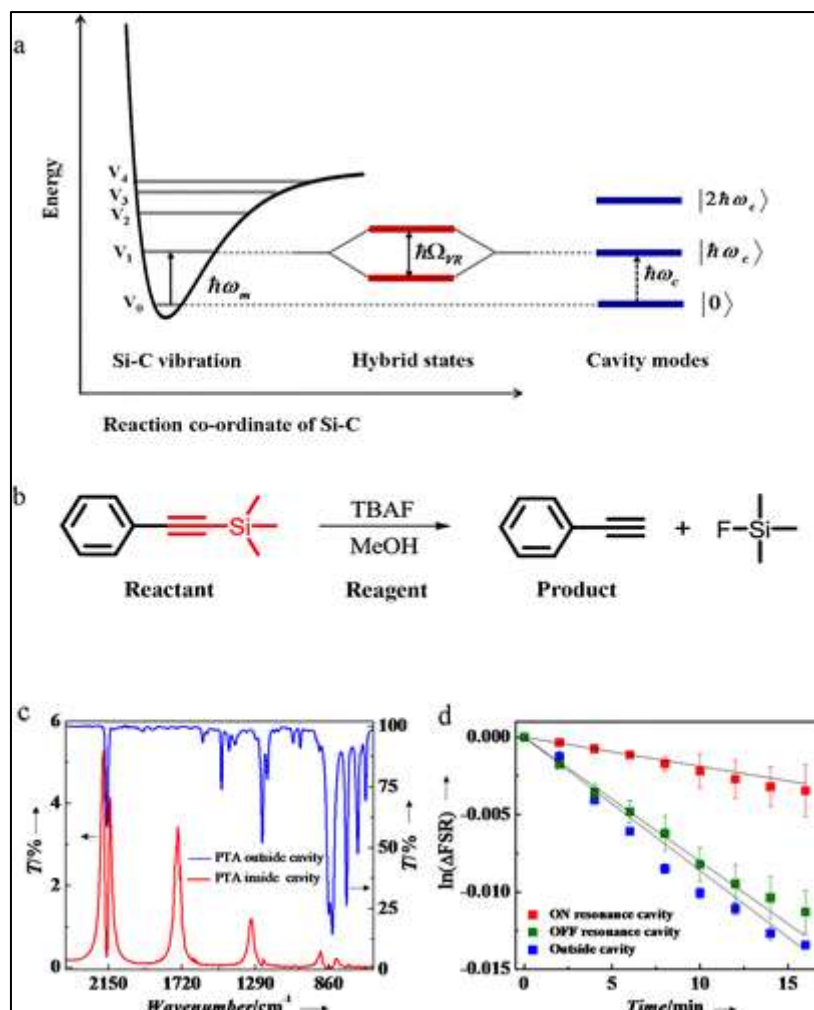


Figure 2.3 (a) Schematic diagram of vibrational strong coupling. b) Deprotection reaction PTA with TBAF (c) IR transmission spectrum of PTA manifesting the coupling at 860 cm^{-1} d) Modification of reaction kinetics through the evolvement of cavity modes in various conditions. The figure is reprinted from [22]

Later, the same group demonstrated non-radiative energy transfer beyond the Forster limit in the donor-acceptor system when strongly coupled to cavity mode²³ In a recent experimental study, Anoop et al. demonstrated that site selectivity of organic reactions to form a particular product can be altered using vibrational strong coupling.²⁴ This particular study reinforced that vibrational strong coupling could modify the ground state chemical reaction landscapes. Recent theoretical shreds of evidences in strong coupling offer the possibilities of modification in potential energy surfaces of various reaction pathways²⁵, altered electron transfer reaction rates²⁶, and modified molecular dynamics through polariton-polariton interactions.²⁷ Polaritonic chemistry investigations spread over a wide range spectrum from studies over plasmonic structures²⁸ and polymers²⁹ to protein structures³⁰ and liquid crystals³¹.

2.2 Vibrational Strong Coupling

Vibrational strong coupling (VSC) is the phenomenon in which the vibrational mode of a molecule is coupled to the cavity mode of vacuum electromagnetic field to form new vibro-polaritonic states (P^+ and P^-).^{32,33} A schematic illustration of vibrational strong coupling is shown in figure 1.6. It is proposed that the strength of bonds formed in the new vibro-polaritonic states will follow the following equation,

$$\omega_v \propto \sqrt{\frac{f}{\mu}}$$

ω_v , f and μ is the vibrational frequency, bond strength and reduced mass of the atoms involved, respectively.

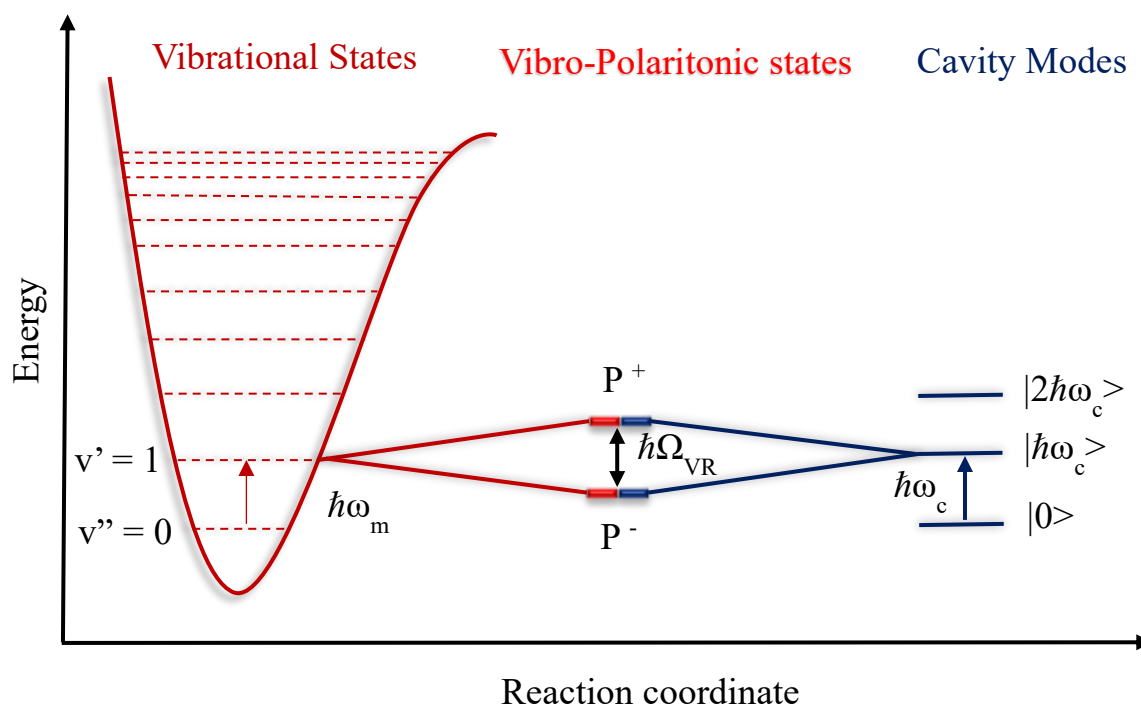


Figure 2.4 Schematic illustration of the vibrational strong coupling phenomenon which forms new vibro-polaritonic states.

Shalabney et al. investigated the coupling of vibrational transitions to the vacuum field for the first time and demonstrated that it is possible to steer the chemical bonds.³² Anoop et al. demonstrated that this phenomenon could modify the reaction mechanism and result in altered chemical reactivity.²² Chemical reaction studies in the VSC regime exhibited acceleration as well as a deceleration in the reaction kinetics.^{34,22} Recently, Hirai et al.

examined a series of reactants undergoing Prins Cyclisation in VSC condition and found a remarkable reduction in reaction rates for all the cases.³⁵ When these solution-based reaction studies were extended to other possibilities like crystallisation, a selective crystal product was obtained under VSC conditions instead of a mixture of products otherwise.³⁶ All these studies undoubtedly reinforce that VSC is an efficient tool to curb chemical reactions efficiently. Even though the experimental, as well as theoretical studies till date, revealed and validated altered chemical reactivity, the exact mechanism of action is still left unanswered.

Wrapping up the whole chapter, strong light-matter interaction which is firmly validated with various experimental as well as theoretical studies paves an exciting way to control chemical reactions and physicochemical properties of materials. Understanding the mechanism of the polaritonic chemistry is the need of the hour. We approached this problem using already proved molecular reactions (here, ester hydrolysis) under cooperative strong coupling condition. The effect of structure-activity relation on ester hydrolysis reaction under vibrational strong coupling condition is discussed in the next chapter.

2.3 Cavity Catalysis and Cooperative Strong Coupling

Recent experiments by Jyoti et. al., on the solvolysis of *para*-nitrophenyl acetate (PNPA) was probed under vibrational strong coupling condition resulted in the enhancement of reaction rate by coupling solvent vibrational band.³⁴ This is specifically achieved by coupling the C=O band of the solvent (ethyl acetate) which has matching vibrational state with the reactant molecules (PNPA). Here, at ON resonance condition, the rate of the reaction is increased by an order of magnitude. This enhancement in the reaction rate is again verified by temperature dependant studies. Thermodynamic studies suggest that both the enthalpy and entropy of activation of the coupled system are decreased and the system still follow Arrhenius relation at room temperature.³⁴ The concept of cooperativity was again validated through solvent kinetic isotope experiments. We exploit the concept of cooperativity to understand the underlying concepts in cavity catalysis and altered behaviour of chemical reactions under vibrational strong coupling.

Experimental Aspects and Implications

Experimental aspects and methodology of strong coupling study of the idea behind this thesis is discussed in this chapter. The chapter starts with an introduction on structure-activity relationship and proceeds with synthesis and characterisations of the molecules involved in the current investigation. In addition, the experimental setup and methodology of achieving strong coupling condition are also discussed. The chapter ends with a discussion on the experimental implications and understandings came out from the investigation.

3.1 Structure-activity Relationship and Hammett Plot

According to transition state theory or activated complex theory of chemical reactions, reactants (R) interact to form an activated complex with higher energy and then stabilise to form a product (P). The highest energy point on the potential energy surface manifests the transition state (TS). Reactants need to cross the activation energy (ΔG^\ddagger) barrier to reach the product state. Transition state theory holds the following proportionality relation,

$$k \propto e^{-\Delta G^\ddagger/RT}$$

where k is the rate constant of the reaction, T is the temperature, ΔG^\ddagger is the activation energy and R is the Boltzmann constant.

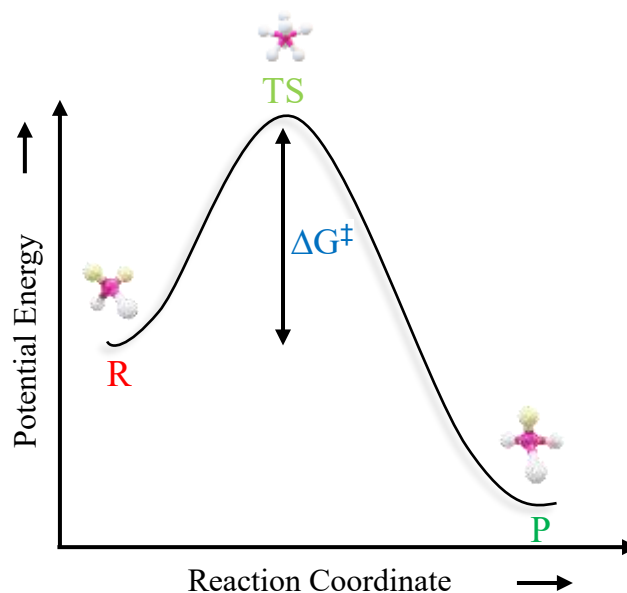


Figure 3.1 Schematic illustration of potential energy surface of a chemical reaction. R denote the reactants, TS denote the transition state, ΔG^\ddagger denote the activation energy and P denote the products.

Understanding the relationship between structure and activity of chemical compounds is a matter of paramount importance to understand the mechanism of organic reactions. One of such salient concepts is the linear Gibbs free energy relationship introduced by L. P. Hammett in 1937.³⁷ He formulated the relationship based on ionisation of meta and para substituted benzoic acids in water at 25°C.

Hammett equation is written as;

$$\text{Log} \left(\frac{K_X}{K_H} \right) = \sigma \rho$$

where K_X denotes the acid constants of meta or para substituted ester and K_H denotes the rate of unsubstituted ester. σ and ρ is termed as substituent constant and reaction constant, respectively.

Substituent constant σ is defined as;

$$\text{Log} \left(\frac{K_X}{K_H} \right)$$

where K_X is the aqueous ionisation constants of meta or para substituted benzoic acids and K_H is the aqueous ionisation constant of unsubstituted benzoic acid. Substituent effect estimates the net polar effect induced at reaction centre by a particular substituent. No matter what is the nature of the reaction, the value of substituent constant at a specific position for a particular substituent remains constant.

Reaction constant (ρ) describes the susceptibility of the reaction centre to various substituents on the benzene ring in comparison to effect induced on the acid dissociation of benzoic acid. In other words, it can be defined as the change in charge density at the transition state during the course of the reaction. ρ value is pulled out from the plot of $\text{Log} \left(\frac{K_X}{K_H} \right)$ vs σ ; slope of this plot gives the ρ value.

Hammett equation takes the following form when rate constants are incorporated,

$$\text{Log} \left(\frac{k_X}{k_H} \right) = \sigma \rho$$

where k_x is the rate constants for variously substituted benzoate esters and k_H is the rate constant for unsubstituted benzoate ester.

3.2 Experimental Setup

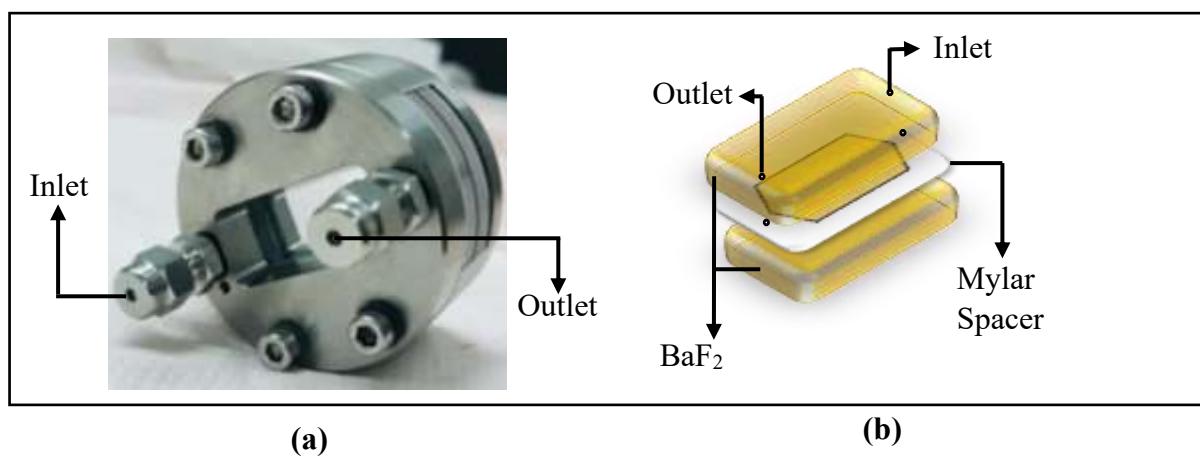
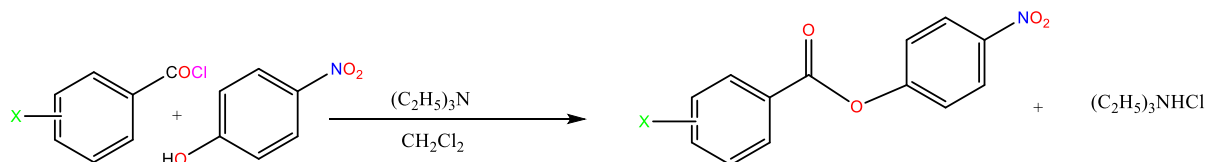


Figure 3.2 a) Image of microfluidic cell used for experiments; b) schematic illustration of a Fabry-Perot cavity.

The experimental setup that we use to study vibrational strong coupling is a Fabry-Perot cavity illustrated in figure 3.2. The mirrors incorporated in the cavity is usually made by substrates like BaF₂, CaF₂, ZnSe, Glass, Quartz etc. These substrates need to be transparent enough to facilitate our probing method. In the current study, we used BaF₂ windows as it is transparent both in IR and UV-VIS region (200 to 10, 000 nm). Each BaF₂ substrate is coated with Au mirrors (10 nm) and are placed one over the other, parallelly by sandwiching a thin film of mylar spacer to create the FP cavity. The distance between the mirrors is adjusted by choosing the right mylar spacer.

3.3 Synthesis of para-nitrophenyl benzoate Esters

All molecules used in the study is synthesized in-situ. Benzoate esters were obtained from the reaction of chosen benzoyl chloride with para-nitrophenol dissolved in dichloromethane in presence of triethylamine for 30 minutes (Scheme1), followed by product separation and recrystallisation from ethanol. All reactions produced good yield. Later, benzoate esters formed were characterised with ¹H NMR (CDCl₃) (Appendix A), FT-IR (Figure 3.4) and melting point (Table 3.2) and validated with literature reports.



Scheme 1

In total, six compounds were synthesized with varied substituents at meta and para positions in the structure shown in figure 3.3. The substituents are X=H, X= m-CH₃, X= p-CH₃, X= m-OCH₃, X= m-Cl, and X= p-Cl.

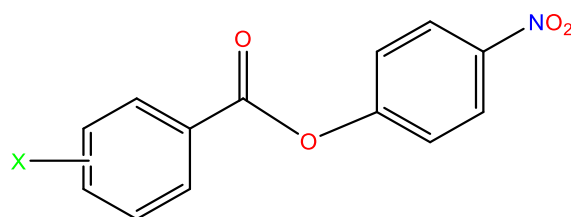


Figure 3.3 Structure of the compound synthesized with varied substituents at meta and para positions. X represents the substituents.

Characterisation Data

p-nitrophenyl benzoate: ¹H NMR (400 MHz, CDCl₃), δ 8.36 (d, *J* = 8.8 Hz, 2H), 8.23 (d, *J* = 7.92 Hz, 2H), 7.71(t, *J* = 7.2 Hz, 1H), 7.57(t, *J* = 7.6 Hz, 2H), 7.45(d, *J* = 8.88 Hz, 2H)

p-nitrophenyl m-toluate: ¹H NMR (400 MHz, CDCl₃), δ 8.35 (d, *J* = 8.84 Hz, 2H), 8.03(d, *J* = 8.2 Hz, 2H), 7.52-7.43(m, 4H), 2.49(s, 3H)

p-nitrophenyl p-toluate: ¹H NMR (400 MHz, CDCl₃), δ 8.34 (d, *J* = 8.76 Hz, 2H), 8.11 (d, *J* = 7.92 Hz, 2H), 7.43 (d, *J* = 8.8 Hz, 2H), 7.36 (d, *J* = 7.92 Hz, 2H), 2.49 (s, 3H)

p-nitrophenyl m-anisate: ¹H NMR (400 MHz, CDCl₃), δ 8.33 (d, *J* = 9.2 Hz, 2H), 7.8(dt, *J* = 8.7 Hz, 1H), 7.68 (dd, *J* = 1.6 Hz, *J* = 2.4 Hz), 7.46-7.4(m, 3H), 7.22 (dddd, *J* = 1.28 Hz, *J* = 3 Hz, *J* = 3.96 Hz, *J* = 8.68 Hz), 3.69 (s, 3H)

p-nitrophenyl m-chlorobenzoate: ¹H NMR (400 MHz, CDCl₃), δ 7.36(d, *J* = 9.16 Hz), 2 H), 8.2 (t, *J* = 1.72 Hz, 1H), 8.11 (dt, *J* = 1.16 Hz, *J* = 2.52 Hz, *J* = 7.82 Hz, 1H), 7.68 (dq, *J* = 1 Hz, *J* = 2.04 Hz, *J* = 3.08 Hz, *J* = 8.04 Hz, 1H), 7.52(t, *J* = 7.92 Hz, 1H), 7.44(d, *J* = 9.12 Hz, 2H)

p-nitrophenyl p-chlorobenzoate: ¹H NMR (400 MHz, CDCl₃), δ 8.35 (d, *J* = 9.2 Hz, 2H), 8.16 (d, *J* = 8.72 Hz, 2H), 7.54 (d, *J* = 7.88 Hz, 2H), 7.44 (d, *J* = 9.2 Hz, 2H)

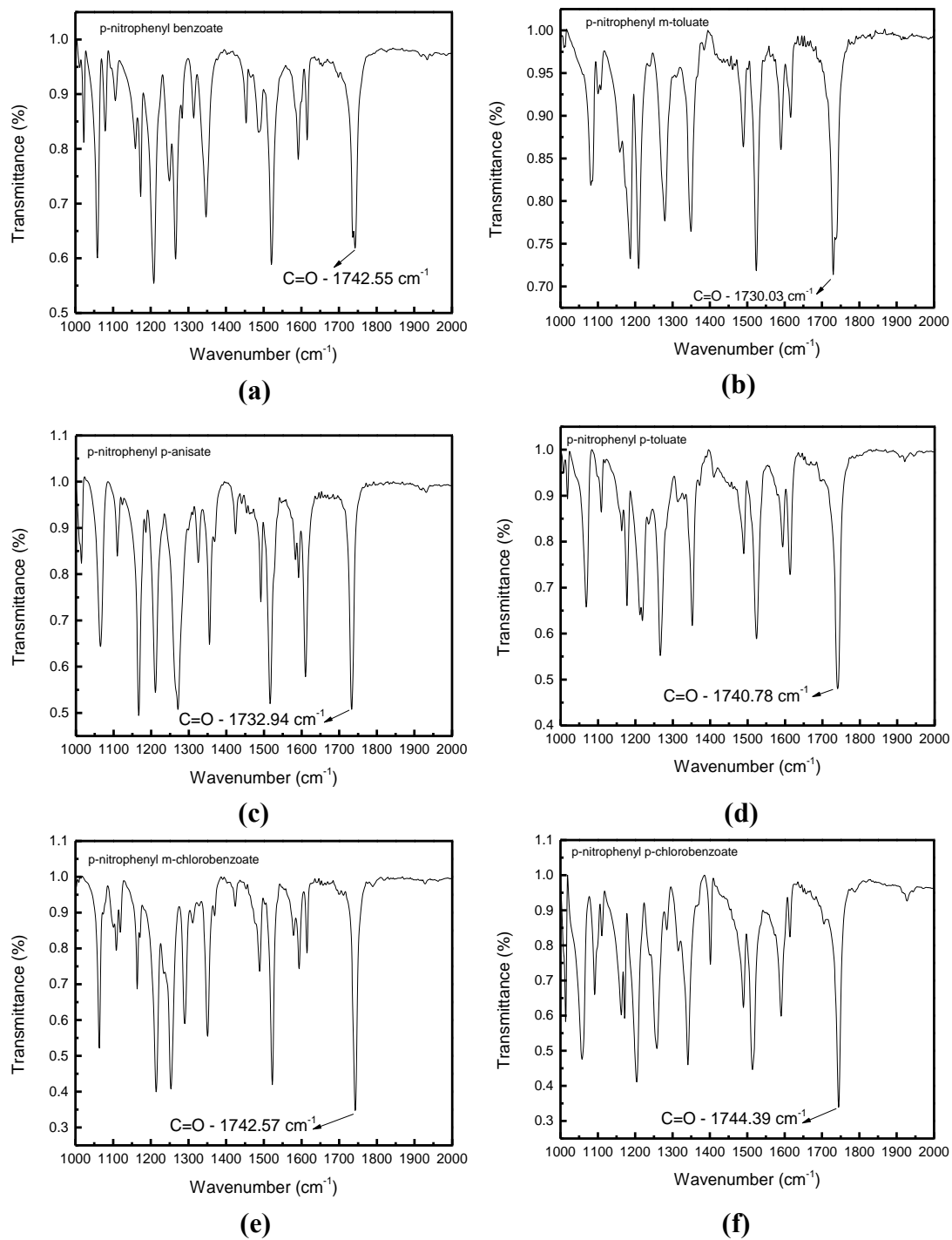


Figure 3.4 Infrared spectrum (KBr) of the benzoate esters. (a) X=H, (b) X= m-CH₃ (c) X= p-CH₃, (d) X= m-OCH₃ (e) X= m-Cl, (f) X= p-Cl.

| Compound | C=O stretching frequency |
|--------------------------------|--------------------------|
| p-nitrophenyl benzoate | 1742.55 cm ⁻¹ |
| p-nitrophenyl m-toluate | 1730.03 cm ⁻¹ |
| p-nitrophenyl p-toluate | 1740.78 cm ⁻¹ |
| p-nitrophenyl m-anisate | 1738.63 cm ⁻¹ |
| p-nitrophenyl m-chlorobenzoate | 1742.57 cm ⁻¹ |
| p-nitrophenyl p-chlorobenzoate | 1744.39 cm ⁻¹ |

Table 3.1 C=O stretching frequency of the benzoate esters.

| Compound | Melting Point (°C) |
|--------------------------------|--------------------|
| p-nitrophenyl benzoate | 143-145 |
| p-nitrophenyl m-toluate | 95-97 |
| p-nitrophenyl p-toluate | 118-120 |
| p-nitrophenyl m-anisate | 113-115 |
| p-nitrophenyl m-chlorobenzoate | 135-137 |
| p-nitrophenyl p-chlorobenzoate | 136-138 |

Table 3.2 Melting point of the molecules synthesized.

3.4 Solvent Systems

As mentioned in the previous section, cooperative VSC is an efficient method to control the chemical reactions. We have chosen ethyl acetate and iso-propyl acetate for studying this cooperative interaction between solvent and reactant molecules. The solvent system was selected in such a way that the C=O stretching mode of the solvent overlap with the reactant C=O vibrational band and this must be valid for all ester derivative synthesised (see the table 3.1 for comparison). The best solvents which match this criteria are isopropyl acetate and ethyl acetate that has a C=O stretching mode at 1734 and 1750 cm⁻¹, respectively.

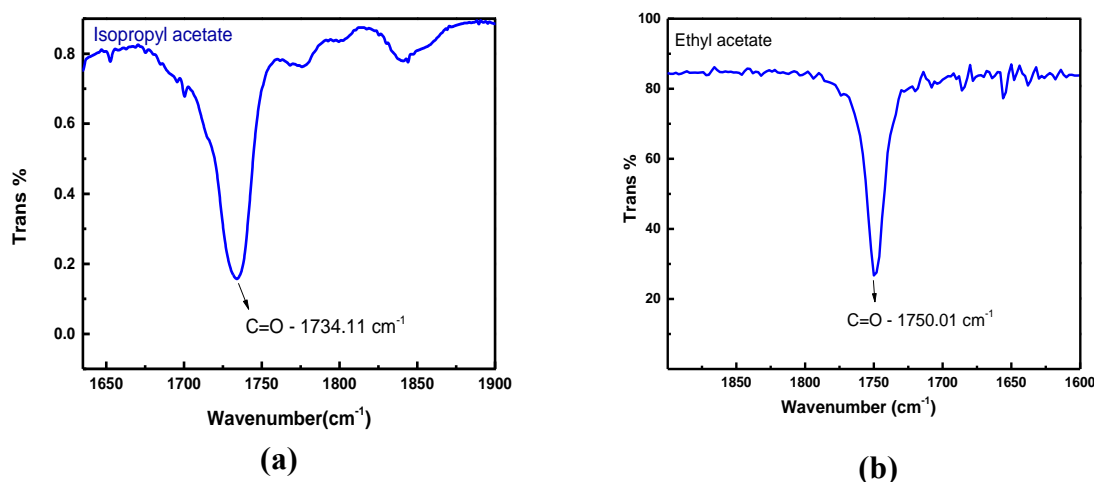


Figure 3.5 a) FT-IR spectrum of isopropyl acetate b) FT-IR spectrum of ethyl acetate.

| Solvent | C=O stretching frequency |
|-------------------|--------------------------|
| Isopropyl Acetate | 1734.11 cm ⁻¹ |
| Ethyl Acetate | 1750.01 cm ⁻¹ |

Table 3.3 C=O stretching frequency of the solvents involved in the study.

3.5 Solvolysis of the benzoate Esters

All reactions are initiated by adding 0.005 M TBAF prepared in methanol to 0.1 M *p*-nitrophenyl benzoate ester prepared in isopropyl acetate. The reaction of *p*-nitrophenyl benzoate ester with TBAF results in the formation of *para*-nitro phenoxide ion which has a λ_{\max} at 407 nm (Figure 3.6).

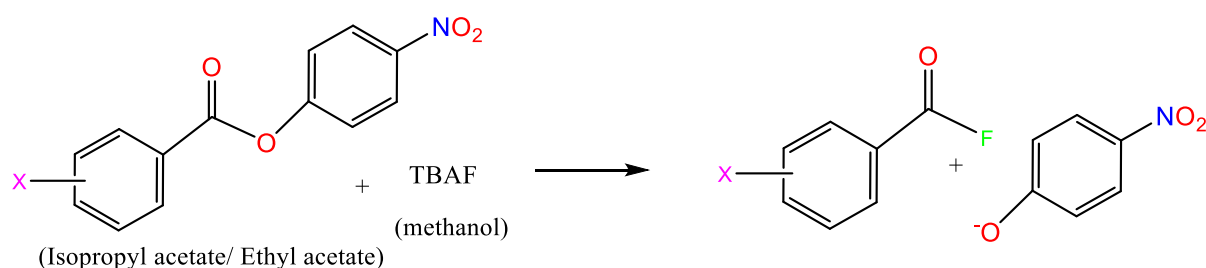


Figure 3.6 Reaction of *para*-nitrophenyl benzoate esters forming *para*-nitro phenoxide ion.

The plausible mechanism for the solvolysis of *para*-nitrophenyl benzoate esters is B_{AC}2 mechanism (base catalysed acyl bond breaking, S_N2). Nucleophilic addition of fluoride anion

to carbonyl centre of the ester forms a tetrahedral intermediate. Since *para*-nitro phenoxide ion is a good leaving group, this reaction follows a concerted reaction path.

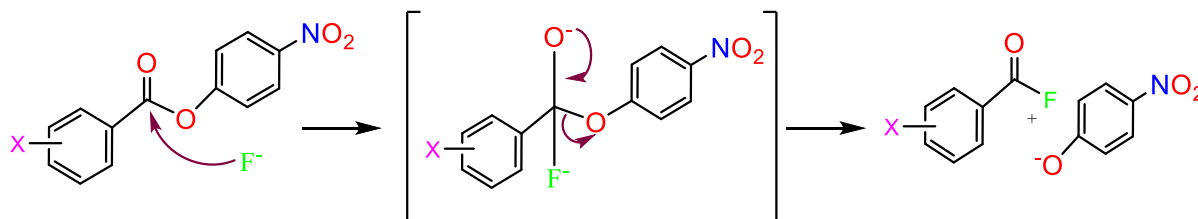


Figure 3.7 Mechanism for the solvolysis of esters.

Solvolysis of the esters follow a pseudo first order kinetics since the esters are present in excess compared to TBAF. The expression for pseudo-first order reaction can be written as,

$$\ln\left(1 - \frac{A_t}{A_f}\right) = k_{app}t$$

where A_t and A_f is the absorbance at time t and at infinity time, respectively. Slope of linear regression plot of $-\ln(1-(A_t/A_f))$ vs time indicate the apparent rate, k_{app} .

3.6 Results and Discussions

Under non-cavity conditions, uncoated BaF_2 windows are used. After placing the BaF_2 windows separated by a mylar spacer of $12 \mu\text{m}$ inside the microfluidic IR cell, the system is stabilised for 30 minutes with a constant temperature of 25°C . Once the system and temperature are stabilised, the reaction initiated outside is immediately injected and kept inside UV-VIS spectrophotometer to monitor (Figure 3.8 (a)). Baseline is recorded just before starting the spectral acquisition. Here, the evolution of the absorption spectra from 350 nm to 500 nm is considered with a time gap of 16 seconds between each spectrum. More precisely, the changes in the absorbance at 407 nm (A_t) indicating the formation of *para*-nitro phenoxide ion is monitored for 10 minutes to assess the progress of the reaction. Apparent rate constants were obtained from linear regression plots (Figure 3.8 (b)).

To determine A_{infinity} of the reaction, solvolysis of *para*-nitro phenyl benzoate is studied under non-cavity condition. The reaction is monitored for 5000 seconds and found the A_{infinity} of the reaction as 0.037 (Figure 3.7). This value of A_{infinity} is used to calculate k_{app} for all other reactions.

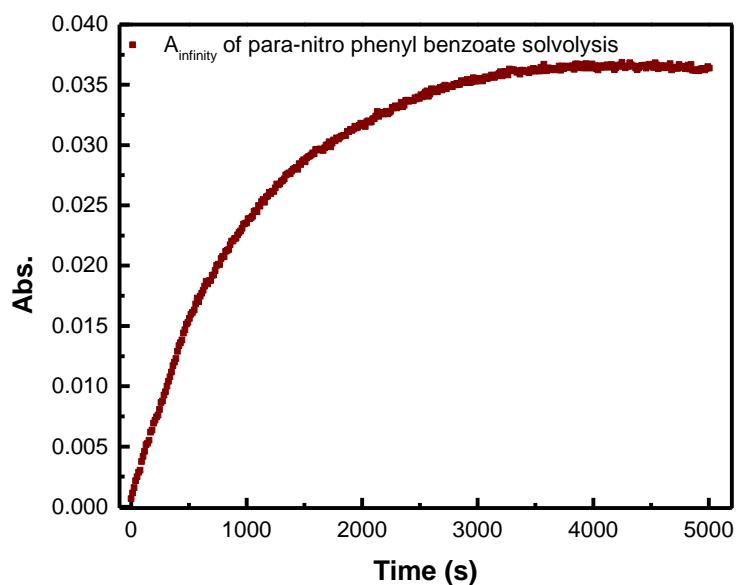


Figure 3.8 Absorbance change for p-nitrophenyl benzoate over time.

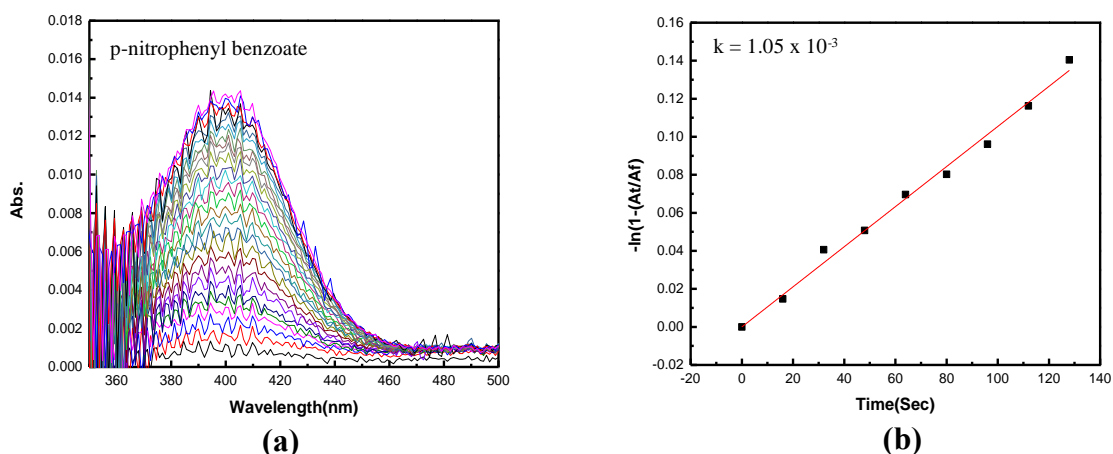


Figure 3.9 (a) Absorption spectra for the solvolysis of para-nitrophenyl benzoate in non-cavity condition in isopropyl acetate. (b) Plot of $-\ln(1-(A_t/A_f))$ vs time to determine the rate of the solvolysis in non-cavity condition.

Apparent rates calculated from the plots in isopropyl acetate and ethyl acetate solvent is tabulated in table 3.2. The k_{app} values of *para*-nitro phenyl benzoate esters substituted with electron-donating groups (m-CH₃, p-CH₃, m-OCH₃) have a lower rate and the para-nitro phenyl benzoate esters substituted with electron-withdrawing groups (m-Cl, p-Cl) have a higher rate in comparison with the unsubstituted one. This contrast in rates clearly manifests the electron-donating and electron-withdrawing effects induced by the substituents at the reaction centre.

| Compound | Isopropyl Acetate k (s ⁻¹) | Ethyl Acetate k (s ⁻¹) |
|--------------------------------|--|------------------------------------|
| p-nitrophenyl benzoate | 1.05 x 10 ⁻³ | 6.83 x 10 ⁻⁴ |
| p-nitrophenyl m-toluate | 7.73 x 10 ⁻⁴ | 1.33 x 10 ⁻⁴ |
| p-nitrophenyl p-toluate | 5.54 x 10 ⁻⁴ | 1.16 x 10 ⁻⁴ |
| p-nitrophenyl m-anisate | 1.19 x 10 ⁻³ | 3.23 x 10 ⁻⁴ |
| p-nitrophenyl m-chlorobenzoate | 1.63 x 10 ⁻³ | 1.1 x 10 ⁻³ |
| p-nitrophenyl p-chlorobenzoate | 1.49 x 10 ⁻³ | 5.65 x 10 ⁻⁴ |

Table 3.4 Apparent rate constants for the solvolysis of esters in the non-cavity condition.

Moreover, a strong dependence of the rates on the solvent can be deciphered from the k values. Even though both solvents have similar polarity index, all reactions exhibited an increased rate of the reaction in isopropyl acetate in comparison with ethyl acetate (Figure 3.9). This increase in the rate can be attributed to the overlap in the IR bands of isopropyl acetate and reactant molecules.

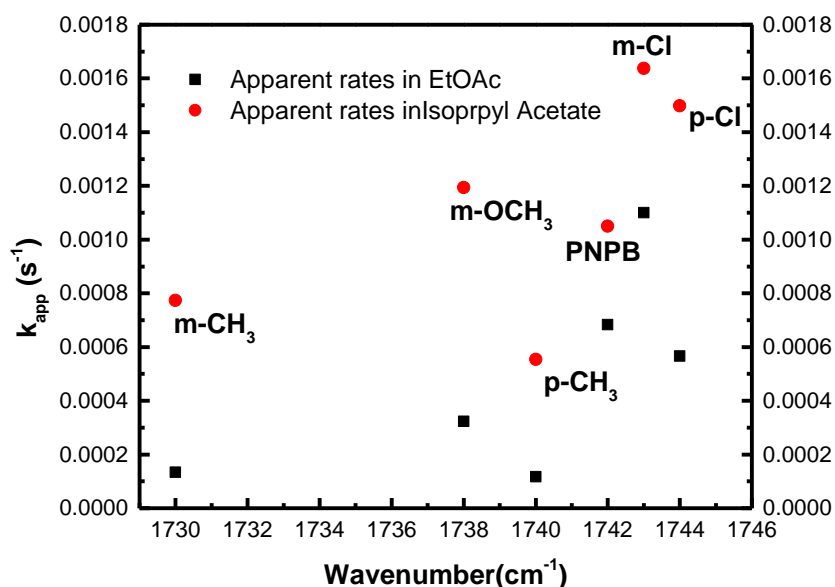


Figure 3.10 Plot depicting the influence of solvent on the rates.

After determining the apparent rates for the solvolysis of all compounds, Hammett correlation is plotted. Sigma values used in Hammett plot are tabulated in table 3.5 and are taken from Ref [38]. Hammett plot indicated a Rho value of 1.8 and .89 for solvolysis in ethyl acetate and isopropyl acetate, respectively. A positive rho value indicates increased electron density in the transition state in comparison with the reactant in the reaction. The increased

positive value in ethyl acetate manifests an increased negative charge development in the transition state in contrast with isopropyl acetate.

| Compound | σ values |
|--------------------------------|-----------------|
| p-nitrophenyl benzoate | 1 |
| p-nitrophenyl m-toluate | -0.07 |
| p-nitrophenyl p-toluate | -0.17 |
| p-nitrophenyl m-anisate | 0.12 |
| p-nitrophenyl m-chlorobenzoate | 0.37 |
| p-nitrophenyl p-chlorobenzoate | 0.23 |

Table 3.5 Substituent constant values used in Hammett plot.

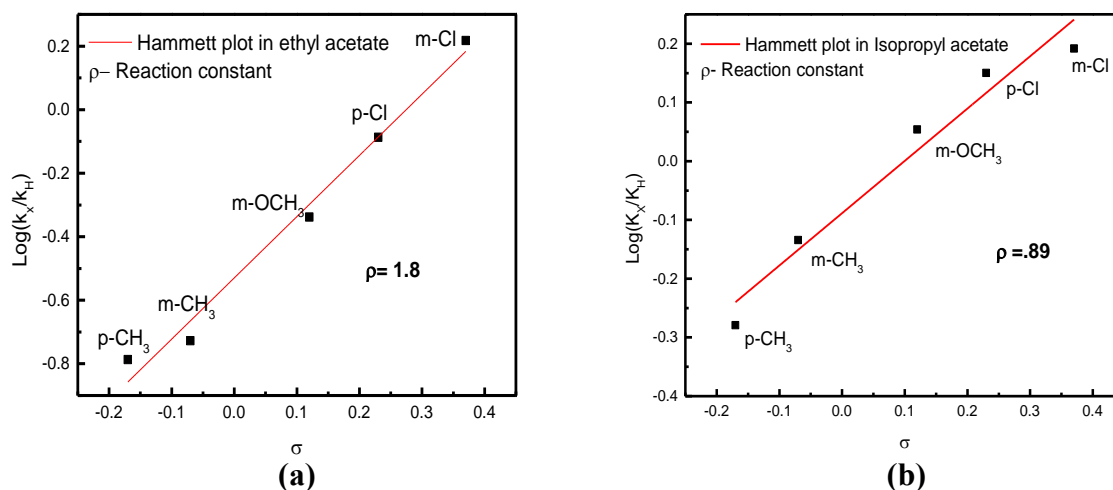


Figure 3.11 Hammett plot in (a) Isopropyl acetate (b) Ethyl acetate under non-cavity conditions.

Cavity experiments were done using BaF₂ windows sputtered with an Au layer of 10 nm. These windows are separated by a mylar spacer of 12 μm inside the flow cell. Optimum path length to form a perfect cavity is obtained by adjusting the screws of flow cell. The formation of cavity modes is observed with an FT-IR spectrophotometer (Figure 3.12 (a)). After obtaining the FSR value facilitating the perfect coupling from back-calculation using the equation $k(\text{cm}^{-1}) = \frac{10000}{2nL}$. Pathlength of the FP cavity is adjusted to obtain the desired cavity mode to couple the C=O stretching band. While calculating the FSR value, an average of 5 cavity modes is considered. FSR values obtained before and after injection of the reaction is

tabulated in table 3.6. After forming a flawless cavity with desired FSR value, it is kept undisturbed for 30 minutes under controlled temperature (25°C). This step is followed by injecting the reaction mixture and keeping inside the U-VIS spectrophotometer to monitor the reaction progress. Baseline is recorded just before starting to record the spectral evolution. Isopropyl acetate has a C=O peak at 1734.11 cm⁻¹ (Figure 3.12 (b)). When this C=O band is coupled to the 7th mode of the cavity, a Rabi splitting energy of 140 cm⁻¹ is obtained. P+ is formed at 1814 cm⁻¹ and P- is formed at 1677cm⁻¹ (Figure 3.12 (b)).

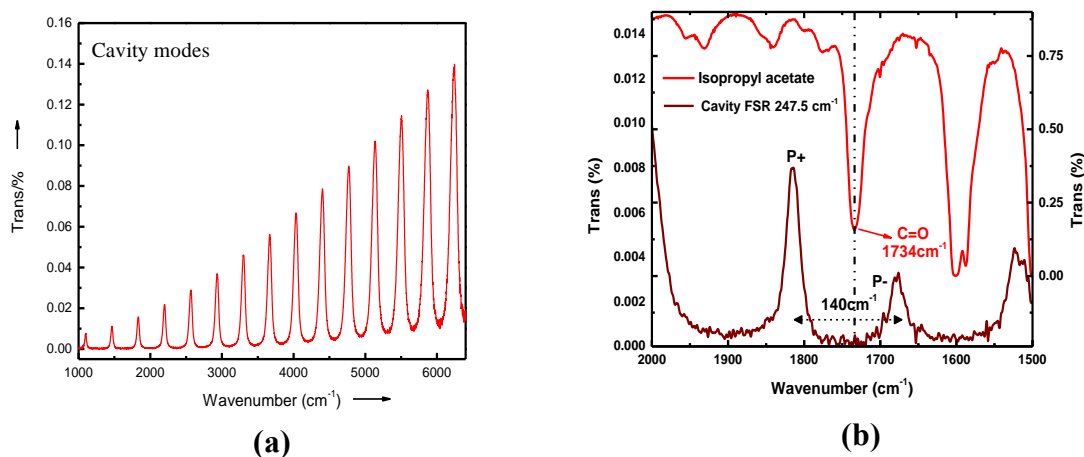


Figure 3.12 (a) Cavity modes formed inside an FP cavity (b) IR spectrum of isopropyl acetate and the corresponding P+ and P- formed by coupling to the 7th mode of the cavity.

| Compound | Empty Cavity FSR | FSR after injection of reaction |
|--------------------------------|------------------|---------------------------------|
| p-nitrophenyl benzoate | 342.676 | 248.857 |
| p-nitrophenyl m-toluate | 339.725 | 246.714 |
| p-nitrophenyl p-toluate | 341.889 | 248.285 |
| p-nitrophenyl m-anisate | 341.299 | 247.857 |
| p-nitrophenyl m-chlorobenzoate | 343.463 | 249.428 |
| p-nitrophenyl p-chlorobenzoate | 343.069 | 249.142 |

Table 3.6 FSR in isopropyl acetate before and after injection in ON-resonance condition.

Spectral evolution and linear regression plot for solvolysis in isopropyl acetate under ON-resonance condition is shown in figure 3.13. Apparent rate constant obtained from linear regression plots under ON-resonance cavity condition are tabulated in table 3.7.

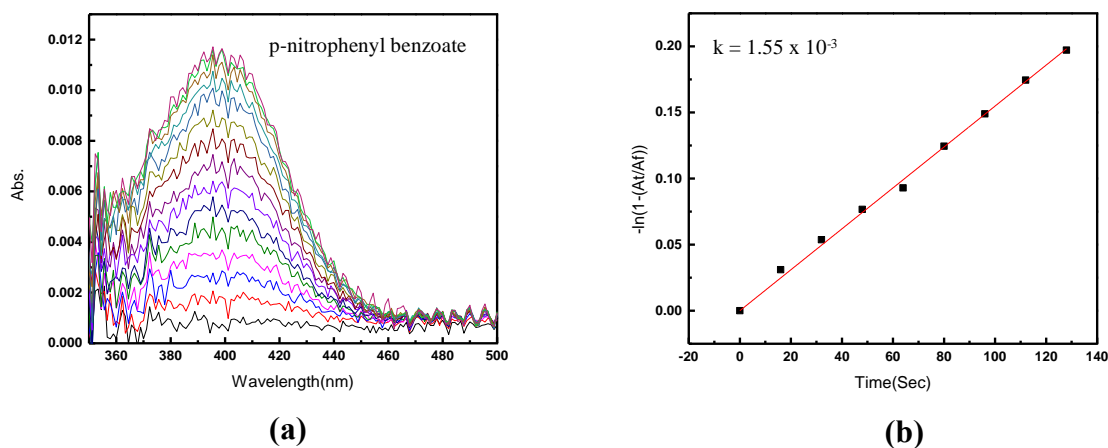


Figure 3.13 (a) Absorption spectra for the solvolysis of para-nitro phenyl benzoate in ON-resonance cavity condition (b) Plot of $-\ln(1-(A_t/A_i))$ vs time to determine the rate of the solvolysis in ON-resonance cavity condition.

| Compound | Non-cavity k (s^{-1}) | Cavity k (s^{-1}) |
|--------------------------------|-----------------------------|-------------------------|
| p-nitrophenyl benzoate | 1.05×10^{-3} | 1.55×10^{-3} |
| p-nitrophenyl m-toluate | 7.73×10^{-4} | 2.58×10^{-3} |
| p-nitrophenyl p-toluate | 5.54×10^{-4} | 1.3×10^{-3} |
| p-nitrophenyl m-anisate | 1.19×10^{-3} | 1.14×10^{-3} |
| p-nitrophenyl m-chlorobenzoate | 1.63×10^{-3} | 2.03×10^{-3} |
| p-nitrophenyl p-chlorobenzoate | 1.49×10^{-3} | 2.19×10^{-3} |

Table 3.7 Apparent rate constants for the solvolysis in isopropyl acetate under non-cavity and cavity condition.

All molecules exhibited modified apparent rate constants for the solvolysis under vibrational strong coupling condition. Except the ester substituted with methoxy group which displayed a comparable apparent rate constant with reference to non-cavity conditions, all other esters exhibited a significant change for apparent rate constants under cavity conditions. Moreover, it can be noted that irrespective of the substituents on the ester, all molecules exhibited an increased apparent rate constant for the solvolysis. Here, it is evident that the slowest reaction shows maximum increase in the apparent rate compared to the fast reactions.

This indicates that partially activation barrier height has a role in rate enhancement under VSC condition³⁹. However, the effect of substituent at the reaction centre has almost no role under VSC as observed in the zero slope of the Hammett plot in figure 3.14. Please note that the reaction under VSC condition shows a large deviation in the (-) ve σ range for this particular reaction. The flat nature of the Hammett plot under VSC has to be understood with more trails of experiments. Here, the substituent effect is feeble as the substituents are far away from the reaction centre, whereas, under VSC this feeble electron density variation may be disappearing due to strong coupling effect.

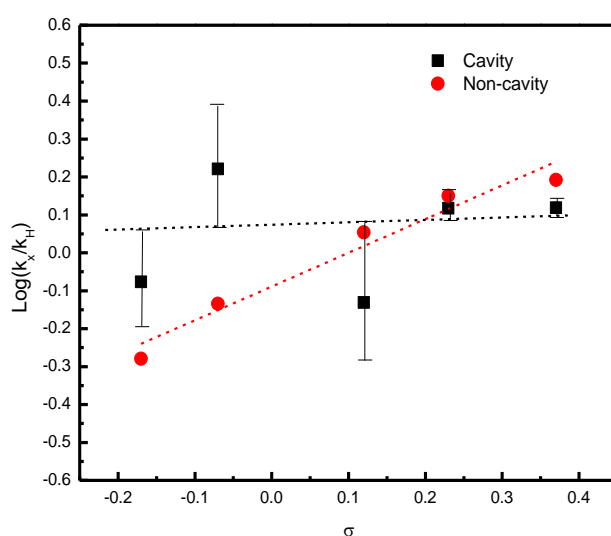


Figure 3.14 Hammett plot in cavity and non-cavity condition when isopropyl acetate is used as the solvent.

3.7 Conclusions

Under non-cavity conditions, apparent rates for the solvolysis of esters manifested a significant dependence on the type of solvent despite similar solvent polarities. Just by adding an isopropyl group, the reaction constant- ρ value doubled for isopropyl acetate in contrary to ethyl acetate. This implies that the electron density (negative character) in the transition state is doubled for solvolysis reaction in isopropyl acetate. When the 7th mode of the cavity is coupled to the C=O band of molecules under cavity conditions, apparent rate constants for the solvolysis of esters varied significantly with respect to non-cavity conditions. This clearly indicates the effect of vibrational strong coupling on the apparent rate constants. Furthermore, the substituent effects at the reaction centre is not that significant under cavity conditions in contrary to the non-cavity conditions. This may be due to a faraway effect of substituents, got

nullified due the VSC at the reaction centre. Further experiments have to be conducted to exactly understand the role VSC in controlling the reaction mechanism and hence the modification of this solvolysis reaction.

Bibliography

1. Purcell, E. M.; Torrey, H. C.; Pound, R. V., Resonance absorption by nuclear magnetic moments in a solid. *Physical review* **1946**, *69* (1-2), 37.
2. Haroche, S.; Kleppner, D., Cavity quantum electrodynamics. *Phys. Today* **1989**, *42* (1), 24-30.
3. Casimir, H. B.; Polder, D., The influence of retardation on the London-van der Waals forces. *Physical Review* **1948**, *73* (4), 360.
4. Lamb Jr, W. E.; Retherford, R. C., Fine structure of the hydrogen atom by a microwave method. *Physical Review* **1947**, *72* (3), 241.
5. Ebbesen, T. W., Hybrid light–matter states in a molecular and material science perspective. *Accounts of chemical research* **2016**, *49* (11), 2403-2412.
6. Yakovlev, V.; Nazin, V.; Zhizhin, G., The surface polariton splitting due to thin surface film LO vibrations. *Optics Communications* **1975**, *15* (2), 293-295.
7. Skolnick, M.; Fisher, T.; Whittaker, D., Strong coupling phenomena in quantum microcavity structures. *Semiconductor Science and Technology* **1998**, *13* (7), 645.
8. Kasprzak, J.; Richard, M.; Kundermann, S.; Baas, A.; Jeambrun, P.; Keeling, J.; Marchetti, F.; Szymańska, M.; André, R.; Staehli, J., Bose–Einstein condensation of exciton polaritons. *Nature* **2006**, *443* (7110), 409-414.
9. Pockrand, I.; Brillante, A.; Möbius, D., Exciton–surface plasmon coupling: An experimental investigation. *The Journal of chemical physics* **1982**, *77* (12), 6289-6295.
10. Lidzey, D. G.; Bradley, D.; Skolnick, M.; Virgili, T.; Walker, S.; Whittaker, D., Strong exciton–photon coupling in an organic semiconductor microcavity. *Nature* **1998**, *395* (6697), 53-55.
11. Fofang, N. T.; Park, T.-H.; Neumann, O.; Mirin, N. A.; Nordlander, P.; Halas, N. J., Plexcitonic nanoparticles: plasmon– exciton coupling in nanoshell– J-aggregate complexes. *Nano letters* **2008**, *8* (10), 3481-3487.
12. Newman, W.; Skinner, A.; Hilbert, S. A., An acoustic demonstration of an avoided crossing. *American Journal of Physics* **2017**, *85* (11), 844-849.
13. Rabi, I., On the process of space quantization. *Physical Review* **1936**, *49* (4), 324.
14. Rabi, I. I., Space quantization in a gyrating magnetic field. *Physical Review* **1937**, *51* (8), 652.
15. Jaynes, E. T.; Cummings, F. W., Comparison of quantum and semiclassical radiation theories with application to the beam maser. *Proceedings of the IEEE* **1963**, *51* (1), 89-109.
16. Purcell, E. M., Spontaneous emission probabilities at radio frequencies. In *Confined Electrons and Photons*, Springer: 1995; pp 839-839.
17. (a) Ciuti, C.; Bastard, G.; Carusotto, I., Quantum vacuum properties of the intersubband cavity polariton field. *Physical Review B* **2005**, *72* (11), 115303; (b) De Liberato, S.; Ciuti, C.; Carusotto, I., Quantum vacuum radiation spectra from a semiconductor microcavity with a time-modulated vacuum Rabi frequency. *Physical review letters* **2007**, *98* (10), 103602.
18. Wang, S.; Mika, A.; Hutchison, J. A.; Genet, C.; Jouaiti, A.; Hosseini, M. W.; Ebbesen, T. W., Phase transition of a perovskite strongly coupled to the vacuum field. *Nanoscale* **2014**, *6* (13), 7243-7248.

19. Katsidis, C. C.; Siapkas, D. I., General transfer-matrix method for optical multilayer systems with coherent, partially coherent, and incoherent interference. *Applied optics* **2002**, *41* (19), 3978-3987.
20. Dyakov, S. A.; Tolmachev, V. A.; Astrova, E. V.; Tikhodeev, S. G.; Timoshenko, V. Y.; Perova, T. S. In *Numerical methods for calculation of optical properties of layered structures*, International Conference on Micro-and Nano-Electronics 2009, International Society for Optics and Photonics: 2010; p 75210G.
21. Hutchison, J. A.; Schwartz, T.; Genet, C.; Devaux, E.; Ebbesen, T. W., Modifying chemical landscapes by coupling to vacuum fields. *Angewandte Chemie International Edition* **2012**, *51* (7), 1592-1596.
22. Thomas, A.; George, J.; Shalabney, A.; Dryzhakov, M.; Varma, S. J.; Moran, J.; Chervy, T.; Zhong, X.; Devaux, E.; Genet, C., Ground-State Chemical Reactivity under Vibrational Coupling to the Vacuum Electromagnetic Field. *Angewandte Chemie* **2016**, *128* (38), 11634-11638.
23. Zhong, X.; Chervy, T.; Zhang, L.; Thomas, A.; George, J.; Genet, C.; Hutchison, J. A.; Ebbesen, T. W., Energy transfer between spatially separated entangled molecules. *Angewandte Chemie International Edition* **2017**, *56* (31), 9034-9038.
24. Thomas, A.; Lethuillier-Karl, L.; Nagarajan, K.; Vergauwe, R. M.; George, J.; Chervy, T.; Shalabney, A.; Devaux, E.; Genet, C.; Moran, J., Tilting a ground-state reactivity landscape by vibrational strong coupling. *Science* **2019**, *363* (6427), 615-619.
25. Kowalewski, M.; Bennett, K.; Mukamel, S., Non-adiabatic dynamics of molecules in optical cavities. *The Journal of chemical physics* **2016**, *144* (5), 054309.
26. Herrera, F.; Spano, F. C., Cavity-Controlled Chemistry in Molecular Ensembles. *Physical Review Letters* **2016**, *116* (23), 238301.
27. Feist, J.; Galego, J.; Garcia-Vidal, F. J., Polaritonic Chemistry with Organic Molecules. *ACS Photonics* **2018**, *5* (1), 205-216.
28. Chikkaraddy, R.; De Nijs, B.; Benz, F.; Barrow, S. J.; Scherman, O. A.; Rosta, E.; Demetriadou, A.; Fox, P.; Hess, O.; Baumberg, J. J., Single-molecule strong coupling at room temperature in plasmonic nanocavities. *Nature* **2016**, *535* (7610), 127-130.
29. Plumhof, J. D.; Stöferle, T.; Mai, L.; Scherf, U.; Mahrt, R. F., Room-temperature Bose–Einstein condensation of cavity exciton–polaritons in a polymer. *Nature Materials* **2014**, *13* (3), 247-252.
30. Dietrich, C. P.; Steude, A.; Tropic, L.; Schubert, M.; Kronenberg, N. M.; Ostermann, K.; Höfling, S.; Gather, M. C., An exciton-polariton laser based on biologically produced fluorescent protein. *Science advances* **2016**, *2* (8), e1600666.
31. Hertzog, M.; Rudquist, P.; Hutchison, J. A.; George, J.; Ebbesen, T. W.; Börjesson, K., Voltage-controlled switching of strong light–matter interactions using liquid crystals. *Chemistry (Weinheim an der Bergstrasse, Germany)* **2017**, *23* (72), 18166.
32. Shalabney, A.; George, J.; Hutchison, J. a.; Pupillo, G.; Genet, C.; Ebbesen, T. W., Coherent coupling of molecular resonators with a microcavity mode. *Nature communications* **2015**, *6* (1), 1-6.
33. George, J.; Chervy, T.; Shalabney, A.; Devaux, E.; Hiura, H.; Genet, C.; Ebbesen, T. W., Multiple Rabi Splittings under Ultrastrong Vibrational Coupling. *Physical Review Letters* **2016**, *117* (15), 153601.

34. Lather, J.; Bhatt, P.; Thomas, A.; Ebbesen, T. W.; George, J., Cavity Catalysis by Cooperative Vibrational Strong Coupling of Reactant and Solvent Molecules. *Angewandte Chemie International Edition* **2019**, *58* (31), 10635-10638.
35. Hirai, K.; Takeda, R.; Hutchison, J. A.; Uji-i, H., Modulation of Prins Cyclization by Vibrational Strong Coupling. *Angewandte Chemie* **2020**, *132* (13), 5370-5373.
36. Hirai, K.; Ishikawa, H.; HUTCHISON, J.; Uji-i, H., Selective Crystallization via Vibrational Strong Coupling. **2020**.
37. Hammett, L. P., Linear free energy relationships in rate and equilibrium phenomena. *Transactions of the Faraday Society* **1938**, *34*, 156-165.
38. Hansch, C.; Leo, A.; Taft, R., A survey of Hammett substituent constants and resonance and field parameters. *Chemical reviews* **1991**, *91* (2), 165-195.
39. Hiura, H.; Shalabney, A., A Reaction Kinetic Model for Vacuum-Field Catalysis Based on Vibrational Light-Matter Coupling. **2019**.

Appendix A

NMR spectra of the p-nitrophenyl benzoate esters

